

Model-independent combination of diphoton constraints at 750 GeV

Jong Soo Kim¹, Krzysztof Rolbiecki^{2,a}, Roberto Ruiz de Austri³

¹ Instituto de Física Teórica, IFT-UAM/CSIC, C/ Nicolás Cabrera, 13-15, Cantoblanco, 28049 Madrid, Spain

² Institute of Theoretical Physics, University of Warsaw, 02093 Warsaw, Poland

³ Instituto de Física Corpuscular, IFIC-UV/CSIC, Valencia, Spain

Received: 16 March 2016 / Accepted: 18 April 2016 / Published online: 2 May 2016
© The Author(s) 2016. This article is published with open access at Springerlink.com

Abstract Motivated by the recent diphoton excess reported by both the ATLAS and CMS collaborations, we provide a model-independent combination of diphoton results obtained at $\sqrt{s} = 8$ and 13 TeV at the LHC. We consider resonant s -channel production of a spin-0 and spin-2 particle with a mass of 750 GeV that subsequently decays to two photons. The size of the excess reported by ATLAS appears to be in a slight tension with other measurements under the spin-2 particle hypothesis.

1 Introduction

The ATLAS and CMS collaboration have found an excess in the search for a diphoton final state after the first 13 TeV data have been analyzed [1,2]. The excess points to a resonance with an invariant mass of about 750 GeV with a local significance of 3.6σ (ATLAS) and 2.6σ (CMS).

The simplest explanation of the excess is through resonant production of a spin-0 or spin-2 particle with a mass of around 750 GeV that decays to photons. A spin-1 resonance is excluded by the Yang–Landau theorem [3,4]. There have been many attempts to explain the excess both via direct production of the 750 GeV resonance or through a heavier particle that decays on-shell to a pair of 750 GeV scalars finally decaying to photons [5–50]; see Ref. [51] for a recent review.

In this letter we investigate whether the interpretation of the diphoton excess via resonant s -channel production is compatible with the full set of Run-I data [52–54] for both the spin-0 and the spin-2 particle hypotheses. We work in a model-independent framework in which we parametrize the diphoton rate by the cross section and branching ratio

to photons and perform a simple statistical test to assess the compatibility between different measurements.

This work is structured as follows. In Sect. 2 we explain the methodology that we have employed, in Sect. 3 we present the results and finally we give our conclusions in the last section.

2 Methodology

We assume that the diphoton signal is resonantly produced,

$$pp \rightarrow X \rightarrow \gamma\gamma, \quad (1)$$

where X denotes either a spin-0 or spin-2 particle. Here, we consider the case where the resonance is only produced via gluon fusion [55],

$$\sigma(pp \rightarrow X) = (2J + 1)\Gamma(X \rightarrow gg) \times \frac{\pi^2}{8m_X^3} \tau \int_{\tau}^1 \frac{dx}{x} g(x, m_X^2) g(\tau, m_X^2), \quad (2)$$

where we have introduced the dimensionless variable $\tau = \frac{m_X^2}{s}$. J and $g(x, m_X^2)$ denotes the spin of the resonance and the gluon distribution function of the proton, respectively. Note that the gluon luminosity ratio between 13 and 8 TeV is 4.7 for $m_X = 750$ GeV [56]. The branching ratio into the diphoton final state is given by

$$\text{BR}(X \rightarrow \gamma\gamma) = \frac{\Gamma(X \rightarrow \gamma\gamma)}{\Gamma(X \rightarrow \gamma\gamma) + \Gamma(X \rightarrow gg) + \Gamma(X \rightarrow YY)}, \quad (3)$$

where Y denotes all other particles which can couple to the resonance X . Due to the much lower increase in the u and d quarks luminosity between $\sqrt{s} = 8$ and 13 TeV of

^ae-mail: krzysztof.rolbiecki@desy.it

Table 1 Selection cuts of the 13 TeV ATLAS/CMS diphoton searches [1,2]

ATLAS	CMS
$p_T(\gamma) \geq 25$ GeV	$p_T(\gamma) \geq 75$ GeV
$ \eta^\gamma \leq 2.37$	$ \eta^\gamma \leq 1.44$ or $1.57 \leq \eta^\gamma \leq 2.5$ at least one γ with $ \eta^\gamma \leq 1.44$
$E_T^{\gamma 1}/m_{\gamma\gamma} \geq 0.4, E_T^{\gamma 2}/m_{\gamma\gamma} \geq 0.3$	$m_{\gamma\gamma} \geq 230$ GeV

2.5–2.7 [13], the production in quark–antiquark annihilation would lead to significant tensions between 8 and 13 TeV results as we will see later. For this reason we will ignore this possibility in the following. This is different for heavy quark initial states: the cross section increase for producing a 750 GeV resonance is 5.1–5.4 for charm and bottom initial states, hence numerically close to the enhancement in gluon–gluon production. Therefore, our results would be qualitatively valid also in this case, albeit with a reduced tension, for a detailed analysis see Ref. [57].¹

A sample of signal events for the spin-0 case was generated with POWHEG [59–61] at the parton level and interfaced with Pythia 6.4 [62] for the parton shower and hadronization with the CTEQ6L1 parton distribution function [63]. A sample for the spin-2 case was generated with Herwig++ 2.7.1 [64] using the MSTW parton distribution functions [65]. For both hypotheses we assume a decay width of 45 GeV. We have implemented the 8 TeV [52–54,66] and 13 TeV [1,2] diphoton searches from ATLAS and CMS into the CheckMATE 1.2.2 framework [67] with its AnalysisManager [68]. CheckMATE 1.2.2 is based on the fast detector simulation Delphes 3.10 [69] with heavily modified detector tunes and it determines the number of expected signal events passing the selection cuts of the particular analysis. The cuts of the ATLAS and CMS analyses are shown in Table 1. We do not follow the approach of both experiments where the expected signal plus background distribution is fitted to the measured $m_{\gamma\gamma}$ distribution. Instead, we just perform a simple cut-and-count study. Our simplified implementation of the analysis certainly leads to a reduced sensitivity, however, our conclusions will still be viable and can be regarded as more conservative. As a result, the signal regions of all employed searches are defined as $700 < m_{\gamma\gamma} < 800$ GeV, except for the ATLAS exotic search [53] where we use the original signal region with $719 < m_{\gamma\gamma} < 805$ GeV. Since the size of the mass bin in the signal regions are relatively large, our conclusions do

not depend on the exact value of the total decay width as long as we do not assume a very broad resonance.

In order to test the implementation of the analyses within the CheckMATE framework we performed a number of tests. For all searches, the acceptance times efficiency is typically provided in the publications and this can be compared to our Monte Carlo (MC) simulation. In Table 2 we compare our efficiency with the efficiency computed by the experimental collaboration. In addition to the efficiency numbers, we provide additional information for each channel. The relative differences between the efficiencies obtained by CheckMATE and the one reported by the experiments are typically around 10%.

The goal is to perform a statistical test of the spin-0 or spin-2 hypothesis taking the 8 and 13 TeV data of the ATLAS and CMS experiment as input, separately as well as combined. The fit was performed with the χ^2 test statistics.² Namely,

$$\chi_i^2 = \frac{(n_i - \mu_i)^2}{\sigma_{i,\text{stat}}^2 + \sigma_{i,b}^2}, \quad (4)$$

where

$$\mu_i = \mu_{i,b} + \mu_{i,s}.$$

Here, n_i is the number of observed events, $\mu_{i,b}$ is the expected number of background events, $\mu_{i,s}$ is the expected number of signal events, $\sigma_{i,\text{stat}}$ and $\sigma_{i,b}$ are the statistical and systematic uncertainty on the expected number of background events for each signal region, i . The total systematic errors combine the systematic errors given by the collaborations (cf. Table 3) and a 10% error on the CheckMATE event yield. For the statistical error we assume that it follows the Poisson distribution.

The fit is performed for three cases: using only ATLAS 13 TeV result; using both measurements at 13 TeV [$i = \text{'ATLAS13'}$, 'CMS13 EBEB' , 'CMS13 EBEE' in Eq. (4)]; and finally using 13 TeV results and exotic searches at 8 TeV [53,66] [$i = \text{'ATLAS13'}$, 'CMS13 EBEB' , 'CMS13 EBEE' , 'ATLAS8 EXO' , 'CMS8 EXO' in Eq. (4)]. We do not combine searches from the same experiment at 8 TeV as these are highly correlated. In the following, we will see that the ATLAS exotic search at $\sqrt{s} = 8$ TeV has a better reach compared to the other 8 TeV diphoton searches. Namely, a potentially higher sensitivity and well defined signal regions which motivated our choice. We use the following conventions for different searches and signal regions: ATLAS13 [1]; CMS13 [2] EBEB, EBEE for the barrel end-cap signal regions; ATLAS8 HIG [52]; ATLAS8 EXO [53]; CMS8 EXO [66]; and CMS8 HIG [54].

¹ It was pointed out in Ref. [58] that the gluon–gluon and $b\bar{b}$ -initiated production could be experimentally distinguishable by looking at p_T distributions of photons and jets as well as a number of additional jets.

² This is reasonable since the number of observed events in most of the signal regions is > 20 .

Table 2 Validation of the CheckMATE implementation of the ATLAS and CMS diphoton searches

Search	Exp. eff. (%)	Comments	CheckMATE (%)	Comments
CMS13 EBEB [2]	34	RS graviton, $m = 750$ GeV	38	RS graviton, $m = 750$ GeV
CMS13 EBEE [2]	22	RS graviton, $m = 750$ GeV	23	RS graviton, $m = 750$ GeV
ATLAS13 [1]	> 40	Scalar, gluon fusion, $m > 600$ GeV	44	Scalar $m = 750$ GeV
ATLAS8 HIG [52]	56–71	Scalar	57	Scalar $m = 750$ GeV
ATLAS8 EXO [53]	50	RS graviton, $m = 2$ TeV	55	RS graviton, $m = 2$ TeV
CMS8 EXO [66]	40	RS graviton, $m = 750$ GeV	45	RS graviton, $m = 750$ GeV
CMS8 HIG [54]	75	Narrow width scalar $m = 750$ GeV	65	Narrow width scalar $m = 750$ GeV

3 Results and discussion

Our results are summarized in Table 3 for the spin-2 resonance and in Table 4 for a spin-0 boson. For each signal region we give the observed number of events, the expected number of background events, its total error and the results for three different fits using different sets of measurements. For example, using the ATLAS13 measurement only, we expect 16.5 signal events for the best-fit point solution which translates to 40.0 signal events in the ATLAS8 EXO search corresponding

to a CL_S value of $8.4 \cdot 10^{-4}$ [70] which is clearly excluded (see columns 4 and 5 of Table 3). Already at this point we can say that the 8 TeV ATLAS result is in tension with other measurements under our model hypothesis.

The results are shown in the $\sigma(pp \rightarrow X)$ -BR($X \rightarrow \gamma\gamma$) plane in Figs. 1, 2, and 3 for the spin-2 resonance. For each point in the cross section and branching ratio plane, we determined the simulated acceptances for all signal regions and we calculated the χ^2 value as given in Eq. (4). Note that for 8 TeV searches the horizontal scale is the same as for

Table 3 The number of events in each signal region for production of a spin-2 particle: observed, SM background, our 'best fit' according to the MC results and the $\Delta\chi^2$ contribution. Each simulated signal region

Signal region	Observed	Background	ATLAS13		ATLAS13+CMS13		Combined	
			Best fit	$\Delta\chi^2$	Best fit	$\Delta\chi^2$	Best fit	$\Delta\chi^2$
ATLAS13	28	11.4 ± 3	16.5	–	6.7	2.7	3.9	4.3
CMS13 EBEB	14	9.5 ± 1.9	16.5	8.2	6.7	0.3	3.9	0.0
CMS13 EBEE	16	18.5 ± 3.7	10.2	5.4	4.1	1.5	2.4	0.8
ATLAS8 HIG	34	28 ± 5	22.4	4.5	9.0	0.2	5.3	0.0
ATLAS8 EXO	99	96.4 ± 3.2	40.0	12.8	16.1	1.7	9.5	0.4
CMS8 EXO	46	48.6 ± 5.4	15.0	4.0	6.1	0.4	3.6	0.1
CMS8 HIG	53	50 ± 6	22.0	4.12	8.9	1.0	5.2	0.5

is compared to three cases, where the best-fit point is obtained using: ATLAS13 data only; CMS13 and ATLAS13 combined; ATLAS and CMS from 8 and 13 TeV combined; see text for details

Table 4 The number of events in each signal region for production of a spin-0 particle: observed, SM background, our 'best fit' according to the simulation results and the $\Delta\chi^2$ contribution. Each simulated signal

Signal region	Observed	Background	ATLAS13		ATLAS13+CMS13		Combined	
			Best fit	$\Delta\chi^2$	Best fit	$\Delta\chi^2$	Best fit	$\Delta\chi^2$
ATLAS13	28	11.4 ± 3	16.6	–	9.6	1.3	6.6	2.7
CMS13 EBEB	14	9.5 ± 1.9	14.4	2.1	8.3	1.1	5.8	0.7
CMS13 EBEE	16	18.5 ± 3.7	5.4	5.6	3.1	0.8	2.2	0.1
ATLAS8 HIG	34	28 ± 5	20.7	3.7	12.0	0.6	8.3	0.1
ATLAS8 EXO	99	96.4 ± 3.2	28.1	5.9	16.2	1.7	11.2	0.7
CMS8 EXO	46	48.6 ± 5.4	12.2	3.7	7.1	1.0	4.9	0.3
CMS8 HIG	53	50 ± 6	21.1	2.9	12.2	1.2	8.4	0.7

region is compared to three cases, where the best-fit point is obtained using: ATLAS13 data only; CMS13 and ATLAS13 combined; ATLAS and CMS from 8 and 13 TeV combined; see text for details

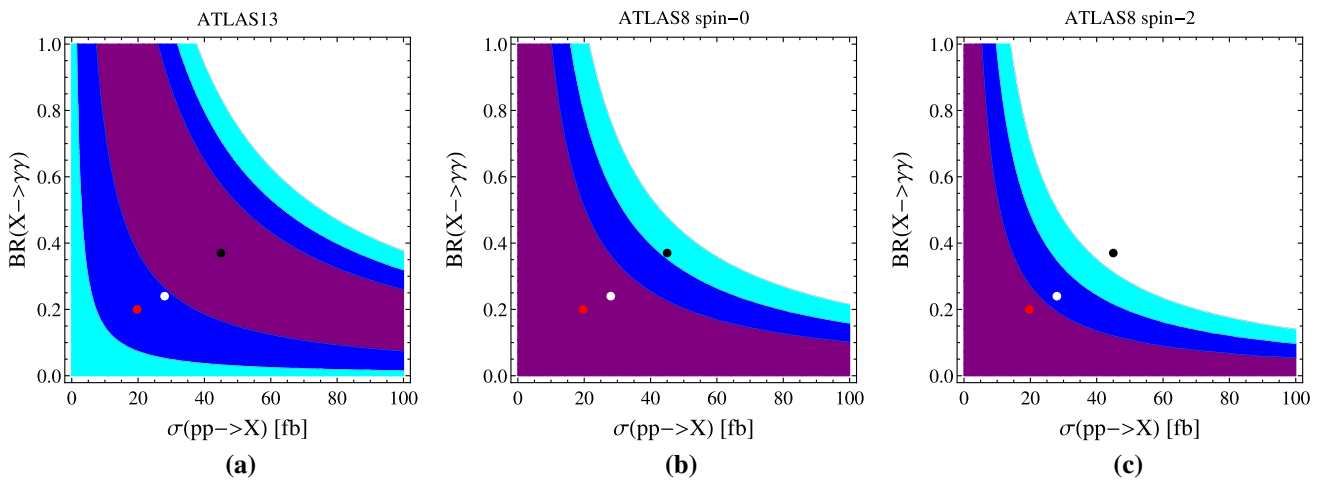


Fig. 1 The distribution of the χ^2 test as a function of $BR(X \rightarrow \gamma\gamma)$ and $\sigma(pp \rightarrow X)$, where X is a spin-2 particle, for **a** ATLAS13 [1]; **b** ATLAS8 HIG [52]; and **c** ATLAS8 EXO [53]. The colors denote: purple 1- σ compatibility; blue 2- σ compatibility; and cyan 3- σ . The dots represent sample best-fit points: the black point corresponds to the fit using only ATLAS13, the white point using both 13 TeV results and the red point for a combination of 8 and 13 TeV

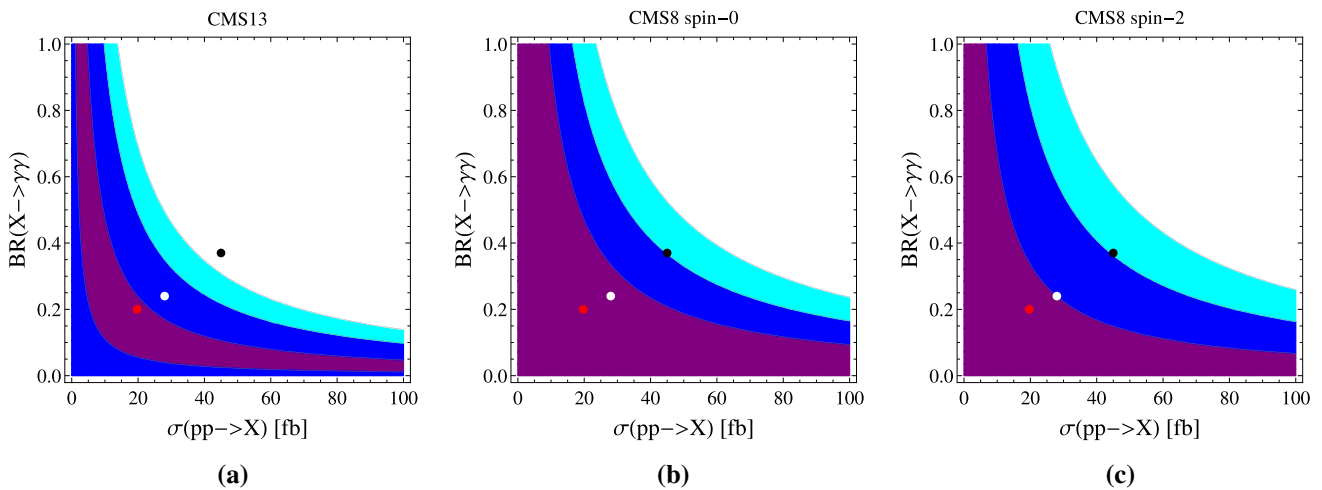


Fig. 2 The distribution of the χ^2 test as a function of $BR(X \rightarrow \gamma\gamma)$ and $\sigma(pp \rightarrow X)$, where X is a spin-2 particle, for **a** CMS13 [2]; **b** CMS8 HIG [54]; and **c** CMS8 EXO [66]. See text and Fig. 1 for more details

13 TeV but in the calculation of the χ^2 and the respective event numbers, the rescaled value is used with the correction factor of 4.7 due to a gluon luminosity ratio between 8 and 13 TeV for a 750 GeV particle [56]. In all plots, different colors denote different level of agreement: purple for 1- σ compatibility, blue for 2- σ , and cyan for 3- σ . In each plot we also show example points that minimize the χ^2 function: the black point corresponds to the fit using only ATLAS13 data, the white point using both 13 TeV results and the red point for a combination of 8 and 13 TeV data. However, one should keep in mind that in each case we obtain a hyperbolic line that minimizes the χ^2 .

In Fig. 1a we show the result of the fit using the ATLAS13 data set. The black point denotes one of the good solutions,

with $\sigma = 45$ fb and $BR(X \rightarrow \gamma\gamma) = 37\%$. This can be compared to the remaining measurements. In case of the ATLAS8 HIG search, Fig. 1b, we see that this point lies just outside the 2- σ contour. When moving to the ATLAS8 EXO search, Fig. 1c, there is a clear tension above 3- σ as was already seen in Table 3. A similar comparison is made for CMS measurements in Fig. 2. Interestingly, it appears that there is also a significant tension between the ATLAS13 and CMS13 measurements. The 8 TeV CMS searches show compatibility at the 2- σ level.

Finally, in Fig. 3a we present a fit to both 13 TeV results. Again, the best-fit point for ATLAS lies between the 2- and 3- σ contours. In Fig. 3b one can see the results of the fit to both 8 and 13 TeV data sets and it is again clearly visible

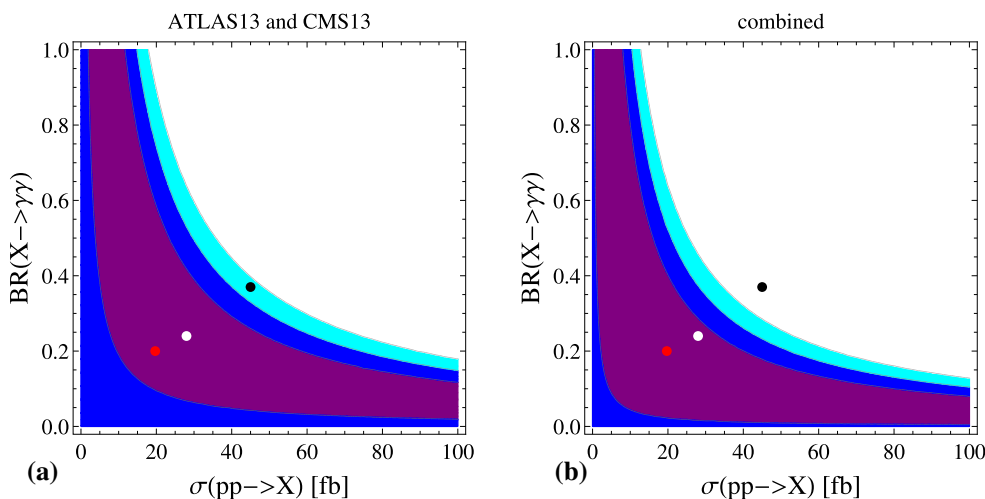


Fig. 3 The distribution of the χ^2 test as a function of $BR(X \rightarrow \gamma\gamma)$ and $\sigma(pp \rightarrow X)$, where X is a spin-2 particle, for **a** combined measurements at 13 TeV ATLAS13 [1] and CMS13 [2], **b** combined mea-

surements at 8 and 13 TeV: ATLAS8 EXO [53], CMS8 EXO [66], ATLAS13 [1], and CMS13 [2]

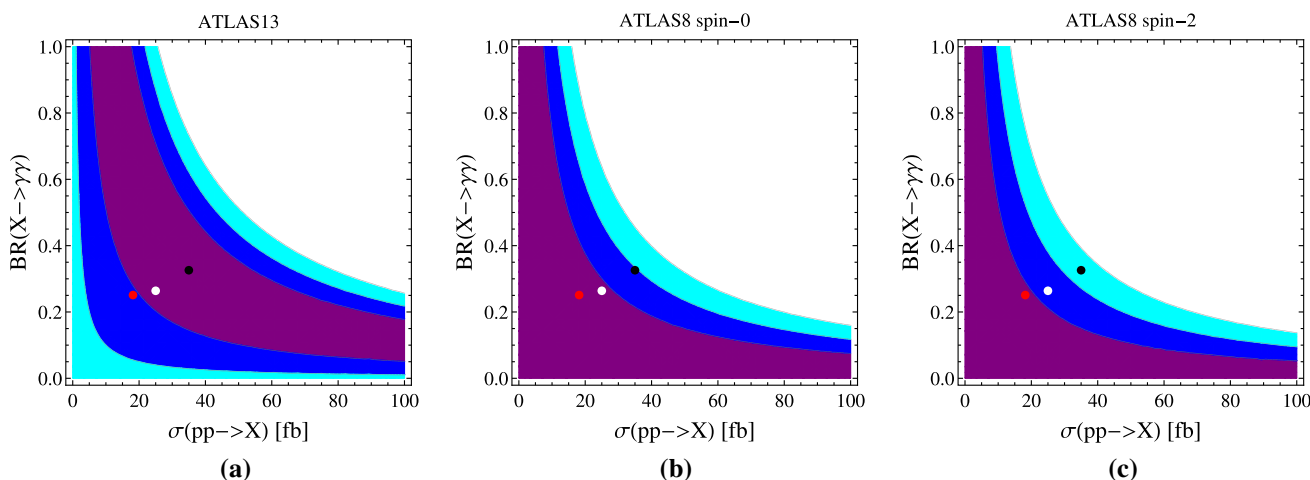


Fig. 4 The distribution of the χ^2 test as a function of $BR(X \rightarrow \gamma\gamma)$ and $\sigma(pp \rightarrow X)$, where X is a spin-0 particle, for **a** ATLAS13 [1]; **b** ATLAS8 HIG [52]; and **c** ATLAS8 EXO [53]. See text and Fig. 1 for more details

that is difficult to accommodate the ATLAS result point with other measurements. However, we want to stress that for the best-fit solution of both 13 TeV results (white point) as well as for the best-fit solution for the combination of 8 and 13 TeV diphoton searches (red point), cf. Eq. (4), the compatibility is within the 1- σ band. Although we considered here only gluon initiated production, the case for quark initiated processes would result in an even bigger tension between 8 and 13 TeV data, since the luminosity ratio for the $q\bar{q}$ initial state is 2.7 [56].

In a similar fashion we also study the production of a spin-0 particle. The results are listed in Table 4 and in Figs. 4, 5 and 6. While the results generally follow a similar pattern as for the spin-2 case, the incompatibility between the

ATLAS13 measurement and the remaining searches is drastically decreased, e.g. the best ATLAS13 fit solution for the spin-0 resonance corresponds to 28.1 signal events in the ATLAS8 EXO search with a $CL_S = 0.02$. The most significant tension can be seen in Fig. 6b where the ATLAS result just lies below the 3- σ contour.

As already mentioned, there is a flat direction in the χ^2 minimum. This is clear since we have several measurements, however, of the same quantity: $\sigma(pp \rightarrow X) \times BR(X \rightarrow \gamma\gamma)$. The degeneracy for the best-fit solution would be lifted by a measurement of the rate of resonance decays into dijet final states. In the following we provide a functional shape of this minimum for each fit considered. The function that reproduces the minimum is given by

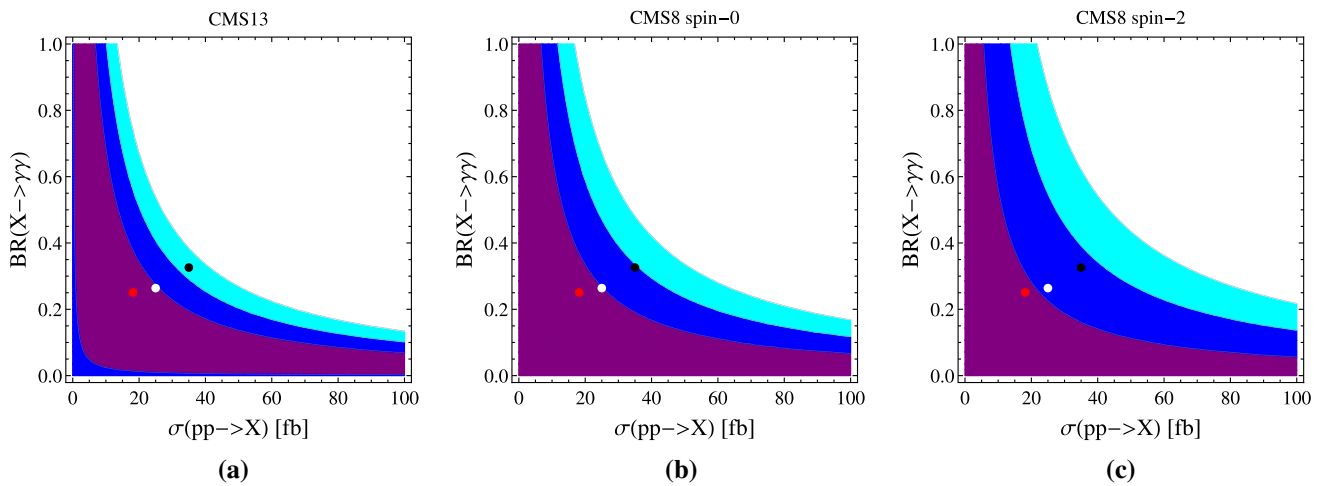


Fig. 5 The distribution of the χ^2 test as a function of $BR(X \rightarrow \gamma\gamma)$ and $\sigma(pp \rightarrow X)$, where X is a spin-0 particle, for **a** CMS13 [2]; **b** CMS8 HIG [54]; and **c** CMS8 EXO [66]. See text and Fig. 1 for more details

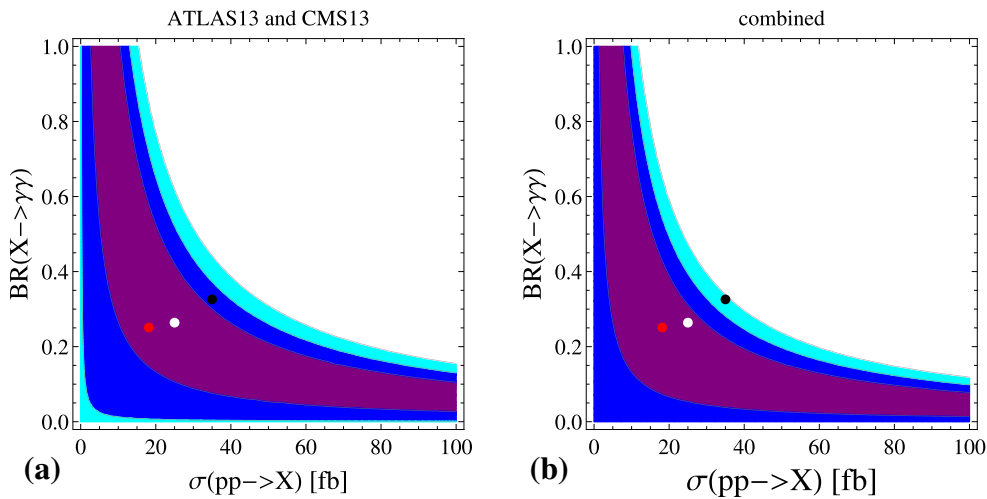


Fig. 6 The distribution of the χ^2 test as a function of $BR(X \rightarrow \gamma\gamma)$ and $\sigma(pp \rightarrow X)$, where X is a spin-0 particle, for **a** combined measurements at 13 TeV ATLAS13 [1] and CMS13 [2] and **b** combined

measurements at 8 and 13 TeV: ATLAS8 EXO [53], CMS8 EXO [66], ATLAS13 [1], and CMS13 [2]

Table 5 The values of the a parameter from Eq. (5) for a spin-2 and spin-0 resonance and different sets of fitted data: only ATLAS13; both measurements at 13 TeV; and the combination of 8 and 13 TeV data

	Spin-2			Spin-0		
	ATLAS13	13 TeV	Combined	ATLAS13	13 TeV	Combined
a [fb]	16.7 ± 6	6.8 ± 3	4.2 ± 2.6	11.4 ± 7	6.0 ± 2.5	4.2 ± 2

$$BR(X \rightarrow \gamma\gamma) = \frac{a}{\sigma(pp \rightarrow X)}, \tag{5}$$

where a is a free parameter and can be determined from the data. The values of a with uncertainties for different cases are summarized in Table 5.

We want to conclude this section with a few comments about other LHC constraints apart from the diphoton searches. In principle, constraints from dijet and diboson

searches could also start to play a role at some point. Regarding the dijet searches, the experimental bounds would typically be at the pb level [71], which is well above the cross sections considered here. Similarly, the diboson searches become relevant for cross sections $\mathcal{O}(100)$ fb [72]. Moreover, those constraints can be avoided depending on exact model assumptions and as a consequence we omit the discussion of other final states.

4 Conclusions

In this work, we have tested the compatibility of the diphoton excess between the ATLAS and CMS diphoton searches at the center-of-mass energies of 8 and 13 TeV. We considered the resonant production of spin-0 and spin-2 particles. We presented our results in a *model-independent* way parametrized in terms of the production cross section and the diphoton branching ratio. The main results of our study are summarized in Tables 3 and 4 as well as in Figs. 3 and 6.

We have found a slight tension between the best-fit solution of the spin-2 scenario for the ATLAS diphoton excess at 13 TeV and the other diphoton searches. In particular, with the exotic search of ATLAS at 8 TeV and the CMS result at 13 TeV where the discrepancy can be larger than $3\text{-}\sigma$ in some cases. However, this tension seems to be significantly smaller for the spin-0 hypothesis.

Finally, we provide a functional form of the relation between the cross section and branching ratio that parametrizes the best fit to the data summarized in Table 3. This can be used in future analyses to quickly find whether the relation predicted in a particular model describes the data well.

Clearly, more data at 13 TeV will be needed to confirm or reject the existence of the excess. We are looking forward to the results of the ongoing Run-II.

Acknowledgments R. RdA is supported by the Ramón y Cajal program of the Spanish MICINN and also thanks the support of the Spanish MICINN's Consolider-Ingenio 2010 Programme under the Grant MULTIDARK CSD2209-00064, the Invisibles European ITN Project (FP7-PEOPLE-2011-ITN, PITN-GA-2011-289442-INVISIBLES) and the "SOM Sabor y origen de la Materia" (FPA2011-29678) and the "Fenomenologia y Cosmologia de la Fisica mas alla del Modelo Estandar e Implicaciones Experimentales en la era del LHC" (FPA2010-17747) MEC Projects. K.R. and J.S.K. has been partially supported by the MINECO (Spain) under contract FPA2013-44773-P; Consolider-Ingenio CPAN CSD2007-00042; the Spanish MINECO Centro de excelencia Severo Ochoa Program under grant SEV-2012-0249; and by JAE-Doc program.

Open Access This article is distributed under the terms of the Creative Commons Attribution 4.0 International License (<http://creativecommons.org/licenses/by/4.0/>), which permits unrestricted use, distribution, and reproduction in any medium, provided you give appropriate credit to the original author(s) and the source, provide a link to the Creative Commons license, and indicate if changes were made. Funded by SCOAP³.

References

1. ATLAS Collaboration, Search for resonances decaying to photon pairs in 3.2 inverse fb of pp collisions at $\sqrt{s} = 13$ TeV with the ATLAS detector, ATLAS-CONF-2015-081
2. CMS Collaboration, Search for new physics in high mass diphoton events in proton-proton collisions at 13 TeV, CMS PAS EXO-15-004
3. L.D. Landau, On the angular momentum of a system of two photons. Dokl. Akad. Nauk Ser. Fiz. **60**(2), 207–209 (1948)
4. C.-N. Yang, Selection rules for the dematerialization of a particle into two photons. Phys. Rev. **77**, 242–245 (1950)
5. K. Harigaya, Y. Nomura, Composite models for the 750 GeV diphoton excess. Phys. Lett. B **754**, 151–156 (2016). [arXiv:1512.04850](https://arxiv.org/abs/1512.04850)
6. Y. Mambrini, G. Arcadi, A. Djouadi, The LHC diphoton resonance and dark matter. Phys. Lett. B **755**, 426–432 (2016). [arXiv:1512.04913](https://arxiv.org/abs/1512.04913)
7. M. Backovic, A. Mariotti, D. Redigolo, Di-photon excess illuminates Dark Matter. JHEP **1603**, 157 (2016). [arXiv:1512.04917](https://arxiv.org/abs/1512.04917)
8. A. Angelescu, A. Djouadi, G. Moreau, Scenarii for interpretations of the LHC diphoton excess: two Higgs doublets and vector-like quarks and leptons. Phys. Lett. B **756**, 126–132 (2016). [arXiv:1512.0492](https://arxiv.org/abs/1512.0492)
9. D. Buttazzo, A. Greljo, D. Marzocca, Knocking on New Physics' door with a Scalar Resonance. Eur. Phys. J. C **76**(3), 116 (2016). [arXiv:1512.0492](https://arxiv.org/abs/1512.0492)
10. S. Knapen, T. Melia, M. Papucci, K. Zurek, Rays of light from the LHC. Phys. Rev. D **93**(7), 075020 (2016). [arXiv:1512.04928](https://arxiv.org/abs/1512.04928)
11. Y. Nakai, R. Sato, K. Tobioka, Footprints of new strong dynamics via anomaly. Phys. Rev. Lett. **116**(15), 151802 (2016). [arXiv:1512.04924](https://arxiv.org/abs/1512.04924)
12. A. Pilaftsis, Diphoton signatures from heavy axion decays at LHC. Phys. Rev. D **93**(1), 015017 (2016). [arXiv:1512.04931](https://arxiv.org/abs/1512.04931)
13. R. Franceschini, G.F. Giudice, J.F. Kamenik, M. McCullough, A. Pomarol, R. Rattazzi, M. Redi, F. Riva, A. Strumia, R. Torre, What is the gamma gamma resonance at 750 GeV?. JHEP **1603**, 144 (2016). [arXiv:1512.04933](https://arxiv.org/abs/1512.04933)
14. S. Di Chiara, L. Marzola, M. Raidal, First interpretation of the 750 GeV di-photon resonance at the LHC. [arXiv:1512.04939](https://arxiv.org/abs/1512.04939)
15. T. Higaki, K.S. Jeong, N. Kitajima, F. Takahashi, The QCD axion from aligned axions and diphoton excess. Phys. Lett. B **755**, 13–16 (2016). [arXiv:1512.05295](https://arxiv.org/abs/1512.05295)
16. S.D. McDermott, P. Meade, H. Ramani, Singlet scalar resonances and the diphoton excess. Phys. Lett. B **755**, 353–357 (2016). [arXiv:1512.05326](https://arxiv.org/abs/1512.05326)
17. J. Ellis, S.A.R. Ellis, J. Quevillon, V. Sanz, T. You, On the Interpretation of a Possible ~ 750 . JHEP **1603**, 176 (2016). [arXiv:1512.05327](https://arxiv.org/abs/1512.05327)
18. M. Low, A. Tesi, L.-T. Wang, A pseudoscalar decaying to photon pairs in the early LHC run 2 data. JHEP **1603**, 108 (2016). [arXiv:1512.05328](https://arxiv.org/abs/1512.05328)
19. B. Bellazzini, R. Franceschini, F. Sala, J. Serra, Goldstones in diphotons. JHEP **1604**, 072 (2016). [arXiv:1512.05330](https://arxiv.org/abs/1512.05330)
20. R.S. Gupta, S. Jaeger, Y. Kats, G. Perez, E. Stamou, Interpreting a 750 GeV diphoton resonance. [arXiv:1512.05332](https://arxiv.org/abs/1512.05332)
21. C. Petersson, R. Torre, The 750 GeV diphoton excess from the goldstino superpartner. Phys. Rev. Lett. **116**(15), 151804 (2016). [arXiv:1512.05333](https://arxiv.org/abs/1512.05333)
22. E. Molinaro, F. Sannino, N. Vignaroli, Strong dynamics or axion origin of the diphoton excess. [arXiv:1512.05334](https://arxiv.org/abs/1512.05334)
23. B. Dutta, Y. Gao, T. Ghosh, I. Gogoladze, T. Li, Interpretation of the diphoton excess at CMS and ATLAS. Phys. Rev. D **93**(5), 055032 (2016). [arXiv:1512.05439](https://arxiv.org/abs/1512.05439)
24. Q.-H. Cao, Y. Liu, K.-P. Xie, B. Yan, D.-M. Zhang, A boost test of anomalous diphoton resonance at the LHC. [arXiv:1512.05542](https://arxiv.org/abs/1512.05542)
25. S. Matsuzaki, K. Yamawaki, 750 GeV diphoton signal from one-family walking technipion. [arXiv:1512.05564](https://arxiv.org/abs/1512.05564)
26. A. Kobakhidze, F. Wang, L. Wu, J.M. Yang, M. Zhang, LHC diphoton excess explained as a heavy scalar in top-seesaw model. Phys. Lett. B **757**, 92–96 (2016). [arXiv:1512.05585](https://arxiv.org/abs/1512.05585)
27. R. Martinez, F. Ochoa, C.F. Sierra, Diphoton decay for a 750 GeV scalar dark matter. [arXiv:1512.05617](https://arxiv.org/abs/1512.05617)
28. P. Cox, A.D. Medina, T.S. Ray, A. Spray, Diphoton excess at 750 GeV from a radion in the Bulk-Higgs scenario. [arXiv:1512.05618](https://arxiv.org/abs/1512.05618)

29. D. Becirevic, E. Bertuzzo, O. Sumensari, R.Z. Funchal, Can the new resonance at LHC be a CP-Odd Higgs boson? *Phys. Lett. B* **757**, 261–267 (2016). [arXiv:1512.05623](#)
30. J.M. No, V. Sanz, J. Setford, See-Saw Composite Higgses at the LHC: linking naturalness to the 750 GeV di-photon resonance. [arXiv:1512.05700](#)
31. S.V. Demidov, D.S. Gorbunov, On sgoldstino interpretation of the diphoton excess. [arXiv: 1512.05723](#)
32. W. Chao, R. Huo, J.-H. Yu, The minimal scalar-stealth top interpretation of the diphoton excess. [arXiv:1512.05738](#)
33. S. Fichet, G. von Gersdorff, C. Royon, Scattering light by light at 750 GeV at the LHC. *Phys. Rev. D* **93**(7), 075031 (2016). [arXiv:1512.05751](#)
34. D. Curtin, C.B. Verhaaren, Quirky explanations for the diphoton excess. *Phys. Rev. D* **93**(5), 055011 (2016). [arXiv:1512.05753](#)
35. L. Bian, N. Chen, D. Liu, J. Shu, A hidden confining world on the 750 GeV diphoton excess. [arXiv:1512.05759](#)
36. J. Chakraborty, A. Choudhury, P. Ghosh, S. Mondal, T. Srivastava, Di-photon resonance around 750 GeV: shedding light on the theory underneath. [arXiv:1512.05767](#)
37. A. Ahmed, B.M. Dillon, B. Grzadkowski, J.F. Gunion, Y. Jiang, Higgs-radion interpretation of 750 GeV di-photon excess at the LHC. [arXiv:1512.05771](#)
38. P. Agrawal, J. Fan, B. Heidenreich, M. Reece, M. Strassler, Experimental considerations motivated by the diphoton excess at the LHC. [arXiv:1512.05775](#)
39. C. Csaki, J. Hubisz, J. Terning, The minimal model of a diphoton resonance: production without Gluon couplings. *Phys. Rev. D* **93**(3), 035002 (2016). [arXiv:1512.05776](#)
40. A. Falkowski, O. Slone, T. Volansky, Phenomenology of a 750 GeV Singlet. *JHEP* **1602**, 152 (2016). [arXiv:1512.05777](#)
41. D. Aloni, K. Blum, A. Dery, A. Efrati, Y. Nir, On a possible large width 750 GeV diphoton resonance at ATLAS and CMS. [arXiv:1512.05778](#)
42. Y. Bai, J. Berger, R. Lu, A 750 GeV Dark Pion: cousin of a dark G-parity-odd WIMP. *Phys. Rev. D* **93**(7), 076009 (2016). [arXiv:1512.05779](#)
43. E. Gabrielli, K. Kannike, B. Mele, M. Raidal, C. Spethmann, H. Veermae, A SUSY inspired simplified model for the 750 GeV diphoton excess. *Phys. Lett. B* **756**, 36–41 (2016). [arXiv:1512.05961](#)
44. R. Benbrik, C.-H. Chen, T. Nomura, Higgs singlet as a diphoton resonance in a vector-like quark model. *Phys. Rev. D* **93**(5), 055034 (2016). [arXiv:1512.06028](#)
45. J.S. Kim, J. Reuter, K. Rolbiecki, R. Ruiz de Austri, A resonance without resonance: scrutinizing the diphoton excess at 750 GeV. *Phys. Lett. B* **755**, 403–408 (2016). [arXiv:1512.06008](#)
46. A. Alves, A.G. Dias, K. Sinha, The 750 GeV S-cion: where else should we look for it?. *Phys. Lett. B* **757**, 39–46 (2016). [arXiv:1512.06091](#)
47. E. Megias, O. Pujolas, M. Quiros, On dilatons and the LHC diphoton excess. [arXiv:1512.06106](#)
48. L.M. Carpenter, R. Colburn, J. Goodman, Supersoft SUSY Models and the 750 GeV diphoton excess, beyond effective operators. [arXiv:1512.06107](#)
49. J. Bernon, C. Smith, Could the width of the diphoton anomaly signal a three-body decay? *Phys. Lett. B* **757**, 148–153 (2016). [arXiv:1512.06113](#)
50. M.R. Buckley, Wide or narrow? The phenomenology of 750 GeV diphotons. [arXiv:1601.04751](#)
51. F. Staub et al., Precision tools and models to narrow in on the 750 GeV diphoton resonance. [arXiv:1602.05581](#)
52. G. Aad et al., ATLAS Collaboration, Search for scalar diphoton resonances in the mass range 65 – 600 GeV with the ATLAS detector in pp collision data at $\sqrt{s} = 8$ TeV, *Phys. Rev. Lett.* **113**(17), 171801 (2014). [arXiv:1407.6583](#)
53. G. Aad et al., ATLAS Collaboration, Search for high-mass diphoton resonances in pp collisions at $\sqrt{s} = 8$ TeV with the ATLAS detector, *Phys. Rev. D* **92**(3), 032004 (2015). [arXiv:1504.05511](#)
54. V. Khachatryan et al., CMS Collaboration, Search for diphoton resonances in the mass range from 150 to 850 GeV in pp collisions at $\sqrt{s} = 8$ TeV, *Phys. Lett. B* **750**, 494–519 (2015). [arXiv:1506.02301](#)
55. V.D. Barger, R.J.N. Phillips, *Collider physics* (1987)
56. L.H.C.S.W. Group, LHC Higgs Cross Section Working Group. <https://twiki.cern.ch/twiki/bin/view/LHCPhysics/CrossSections>
57. F. Domingo, S. Heinemeyer, J.S. Kim, K. Rolbiecki, The NMSSM lives—with the 750 GeV diphoton excess. [arXiv:1602.07691](#)
58. J. Bernon, A. Goudelis, S. Kraml, K. Mawatari, D. Sengupta, Characterising the 750 GeV diphoton excess. [arXiv:1603.03421](#)
59. P. Nason, A new method for combining NLO QCD with shower Monte Carlo algorithms. *JHEP* **11**, 040 (2004). [arXiv:hep-ph/0409146](#)
60. S. Frixione, P. Nason, C. Oleari, Matching NLO QCD computations with Parton Shower simulations: the POWHEG method. *JHEP* **11**, 070 (2007). [arXiv:0709.2092](#)
61. S. Alioli, P. Nason, C. Oleari, E. Re, A general framework for implementing NLO calculations in shower Monte Carlo programs: the POWHEG BOX. *JHEP* **06**, 043 (2010). [arXiv:1002.2581](#)
62. T. Sjostrand, S. Mrenna, P.Z. Skands, PYTHIA 6.4 Physics and Manual, *JHEP* **05**, 026 (2006). [arXiv:hep-ph/0603175](#)
63. H.-L. Lai, M. Guzzi, J. Huston, Z. Li, P.M. Nadolsky, J. Pumplin, C.P. Yuan, New parton distributions for collider physics. *Phys. Rev. D* **82**, 074024 (2010). [arXiv:1007.2241](#)
64. M. Bahr et al., Herwig++ physics and manual. *Eur. Phys. J. C* **58**, 639–707 (2008). [arXiv:0803.0883](#)
65. A.D. Martin, W.J. Stirling, R.S. Thorne, G. Watt, Parton distributions for the LHC. *Eur. Phys. J. C* **63**, 189–285 (2009). [arXiv:0901.0002](#)
66. CMS Collaboration, Search for high-mass diphoton resonances in pp collisions at $\sqrt{s} = 8$ TeV with the CMS detector, *Tech. Rep. CMS-PAS-EXO-12-045* (CERN, Geneva, 2015)
67. M. Drees, H. Dreiner, D. Schmeier, J. Tattersall, J.S. Kim, CheckMATE: Confronting your Favourite New Physics Model with LHC Data. *Comput. Phys. Commun.* **187**, 227–265 (2014). [arXiv:1312.2591](#)
68. J.S. Kim, D. Schmeier, J. Tattersall, K. Rolbiecki, A framework to create customised LHC analyses within CheckMATE, *Comput. Phys. Commun.* **196**, 535–562 (2015). [arXiv:1503.01123](#)
69. J. de Favereau, C. Delaere, P. Demin, A. Giammanco, V. Lemaître, A. Mertens, M. Selvaggi, DELPHES 3 Collaboration, DELPHES 3, A modular framework for fast simulation of a generic collider experiment, *JHEP* **02**, 057 (2014). [arXiv:1307.6346](#)
70. A.L. Read, Presentation of search results: the CL(s) technique, *J. Phys. G* **28**, 2693–2704 (2002) [11 (2002)]
71. G. Aad et al., ATLAS Collaboration, Search for new phenomena in the dijet mass distribution using $p - p$ collision data at $\sqrt{s} = 8$ TeV with the ATLAS detector, *Phys. Rev. D* **91**(5), 052007 (2015). [arXiv:1407.1376](#)
72. G. Aad et al., ATLAS Collaboration, Combination of searches for WW , WZ , and ZZ resonances in pp collisions at $\sqrt{s} = 8$ TeV with the ATLAS detector, *Phys. Lett. B* **755**, 285–305 (2016). [arXiv:1512.05099](#)